KV_6O_{11}: A magnetic metal synthesized at high pressure

Yasushi Kanke
National Institute for Research in Inorganic Materials, 1-1 Namiki, Tsukuba, Ibaraki 305-0044, Japan
(Received 17 December 1998)

An AV_6O_{11}-type magnetic metal KV_6O_{11} was discovered by a high-pressure synthesis. It crystallizes in hexagonal $P6_3/mmc$ at 295 K, whereas in hexagonal $P6_3mc$ at 154 K. KV_6O_{11} shows three magnetic transitions at 190, 66.8, and 35.1 K. KV_6O_{11} is paramagnetic above 66.8 K. Its inverse magnetic susceptibility is slightly concave upward with respect to temperature above 190 K, but the relationship is significantly concave upward below 190 K. KV_6O_{11} shows uniaxial magnetic anisotropy with an easy axis of magnetization parallel to the [001] direction below 66.8 K. The magnetization shows an anomaly at 35.1 K. The resistivity normal to [001] is of the order of $10^{-4}\,\Omega\,\mathrm{cm}^{-1}$. The resistivity versus temperature shows a positive slope above 190 K, a broad maximum at around 90 K, a linear relationship with a positive slope between 35.1 and 66.8 K, and Fermi-liquid-type behavior below 35.1 K. The paramagnetic state below 190 K is discussed on the basis of two types of spin-gap models. Problems of the models are also pointed out. The saturated magnetization versus temperature shows a hyperbolic relationship. The magnetization cannot be explained by the well-known mean field theory or the spin fluctuation mechanism. [S0163-1829(99)01630-6]

I. INTRODUCTION

Various V^{3+}-V^{4+} mixed valence oxides show metal-insulator transitions as functions of temperature. They are relevant substances to understand the nature of $3d$ electrons in states between localized and itinerant. A series of hexagonal V^{3+}-V^{4+} oxides, AV_6O_{11} [A=Na (Ref. 1) Sr (Ref. 2) Pb (Ref. 3)] have become of interest because of their unusual magnetism, electric conductivity, and structural phase transitions.[4–15]

NaV_6O_{11} is paramagnetic above 64.2 K ($=T_C$).[5] Its magnetic susceptibility χ obeys the Curie-Weiss law above 240 K ($=T_t$), but below T_t.[5] NaV_6O_{11} shows uniaxial magnetic anisotropy with an easy axis of magnetization parallel to [001] below T_C.[5] The resistivity of NaV_6O_{11} is also anisotropic.[4,5] In what follows, $\rho_\parallel$ and $\rho_\perp$ represent resistivity parallel to [001] and that perpendicular to [001], respectively. Between 5 and 300 K, $\rho_\parallel$ shows normal metallic character without any anomaly. $\rho_\parallel$ is of the order of 10^{-5}–$10^{-6}\,\Omega\,\mathrm{cm}$, and $\partial\rho_\parallel/\partial T$ is positive, whereas $\rho_\perp$ is approximately one order of magnitude larger than $\rho_\parallel$ and shows anomalies at T_C, T_t, and 80 K.

AV_6O_{11} compounds are essentially isostructural with $BaTi_2Fe_4O_{11}$,[16–18] $BaSn_2Fe_4O_{11}$,[18,19] and $BaFe_2Ru_4O_{11}$.[20] A homologous structure of the spinel structure and AV_6O_{11} one corresponds to the magnetoplumbite structure (Fig. 1). $BaFe_{12}O_{19}$ (Refs. 21 and 22) and $NaFe_3V_9O_{19}$, (Ref. 23–25) crystallize in magnetoplumbite type. The former is a well-known permanent magnet material, and the latter shows spontaneous magnetization below 240 K. AV_6O_{11} phases consist of three types of V atoms, $V(1)O_6$ and $V(2)O_6$ octahedra and $V(3)O_5$ trigonal bipyramid. The $V(1)O_6$ octahedra form a *kagomé* lattice normal to the hexagonal [001] direction by edge sharing. The $V(2)O_6$ octahdedra form a face-sharing dimer parallel to [001]. NaV_6O_{11} crystallizes in hexagonal $P6_3/mmc$ above T_t, in hexagonal $P6_3mc$ between 80 K and T_t, and in orthorhombic $Cmc2_1$ below 80 K.[7–9,15] The $P6_3/mmc$-$P6_3mc$ transition is of second order, and the $P6_3mc$-$Cmc2_1$ transition is of first order.[8,14] The V(1) *kagomé* lattice consists of a unique regular triangle in the $P6_3/mmc$ phase. In the $P6_3mc$ phase, the triangle maintains regularity, but branches into larger and smaller types, and the V(1) atoms form a *kagomé* trimer. In the $Cmc2_1$ phase, the shape of the *kagomé* trimer is transformed into an isosceles triangle, and the V(1) atoms branch into two types. A pair of the V(2) atoms forming the dimer are no longer equivalent in both $P6_3mc$ and $Cmc2_1$ phases. The V(3) atoms are unique in all of the three phases.

Two ^{51}V NMR absorption peaks of NaV_6O_{11} are detected at 300 K.[6] One exhibits a small Knight shift, -0.1%, and the shift is almost independent of temperature. The Knight shift of the other is -2% at 300 K, and the negative shift in-

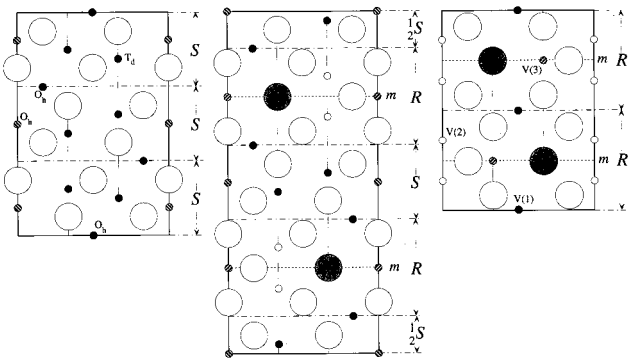

FIG. 1. (111) sectional view of cubic Fe_3O_4 (left) and (110) sectional views of hexagonal $BaFe_{12}O_{19}$ (middle) and hexagonal NaV_6O_{11} (right). *S* and *R* represent spinel block and *R* block, respectively. Thin vertical lines and dashed horizontal lines (*m*) indicate threefold axes and mirror planes, respectively. Large open circles, large shaded circles, and small circles indicate O atoms, Ba or Na atoms, and Fe or V atoms, respectively. Patterns in small circles represent types of the Fe/V atoms. Two types of the octahedral Fe sites in Fe_3O_4 are equivalent due to the cubic crystal system.

creases on cooling. The latter peak split into two in the $P6_3mc$ state. A zero-field ^{51}V NMR study of NaV_6O_{11} at 4.2 K detected three lines, but without assignment so far.[10]

The paramagnetic state of SrV_6O_{11} shows qualitatively the same behavior as that of NaV_6O_{11}, showing a transition at 320 K ($=T_t$).[6] However, SrV_6O_{11} is insulating in its magnetically ordered state below 70 K ($=T_C$) and shows metamagnetism below 35 K.[6] The crystal structure of SrV_6O_{11} at room temperature was described in $P6_3/mmc$ with rather high R factors.[7] Recently, the $P6_3/mmc$-$P6_3mc$ transition has been observed between room temperature and 353 K,[26,27] as in the case with NaV_6O_{11}.

PbV_6O_{11} is paramagnetic above 90 K ($=T_C$).[13,28] Its χ shows qualitatively same temperature dependence as those of NaV_6O_{11} and SrV_6O_{11} with an anomaly at 560 K ($=T_t$).[28] PbV_6O_{11} exhibits spin-glass-type behavior with a freezing temperature of 50 K and is insulating below 50 K.[13] It crystallizes in $P6_3mc$ at room temperature.[13]

The three AV_6O_{11} compounds exhibit a common character at their paramagnetic states, but, especially NaV_6O_{11}, show drastic differences below T_C. An itinerant electron model is proposed for NaV_6O_{11}.[12] The model attributes the spontaneous magnetization of NaV_6O_{11} to spin polarization. However, the origin of their unusual magnetism has not been revealed so far.

The three AV_6O_{11} compounds are synthesized at ambient pressure whose A and O atoms form hexagonal close packed layers. Trials to prepare AV_6O_{11}(A=Ca, Ba, La, Nd, Bi, Tl) at ambient pressure have failed.[2,13] High-pressure synthesis would be relevant to dense packing and simple and high-symmetrical crystal structures. The characters would be advantageous to magnetic order and metallic conductivity. In this study, KV_6O_{11} is prepared at 5.5–6.0 GPa and at 1473–2273 K. The structural phase transition, magnetism, and electric conductivity of KV_6O_{11} are studied.

II. EXPERIMENT

A. Synthesis

The starting materials V_2O_5 (99.9%) and K_2CO_3 (99.9%) were dried at 873 and 573 K immediately before using, respectively. V_2O_3 was prepared by reducing V_2O_5 in a H_2/N_2 atmosphere at 1073 K for 2 h. V_2O_4 was obtained by heating an equimolar mixture of V_2O_5 and V_2O_3 in a sealed silica tube at 1273 K for 3 days. KVO_3 was synthesized by heating an equimolar mixture of K_2CO_3 and V_2O_5 at 773 K for 5 days with several intermediate grindings.

High-pressure synthesis was performed at 5.5–6.0 GPa and at 1473–2273 K using two belt-type presses, FB30H (Ref. 29) with a bore diameter of 32 mm and FB40H with that of 44 mm. The pressure was calibrated at room temperature by means of the known pressure-induced phase transitions in Bi, Tl, and Ba.[30,31] The temperature was estimated from the extrapolated relations between the input electric power and the temperature, which had been obtained in advance by measuring the temperature up to 1773–2073 K with a W(5% Re)-W(26% Re) thermocouple.[30,31] The pressure effect on the electromotive force of the thermocouple was not corrected.

About 0.3 g (for FB30H) or about 2.5 g (for FB40H) of a mixture of KVO_3, V_2O_3, and V_2O_4 was mechanically sealed in a platinum capsule. Two capsules were assembled in a cell with a graphite heater (Fig. 2). The assembly for higher temperature was modified to maintain temperature stability.[30,31] The cell was pressed at the target pressure and heated at 1573 K for 60–120 min (preliminary study) or for 5–10 min to wait melting the sodium chloride inside the graphite heater (crystal synthesis). For crystal synthesis, the temperature was then increased to the target temperature. Finally, the cell was quenched to room temperature and was gradually released to ambient pressure to avoid a blowout.

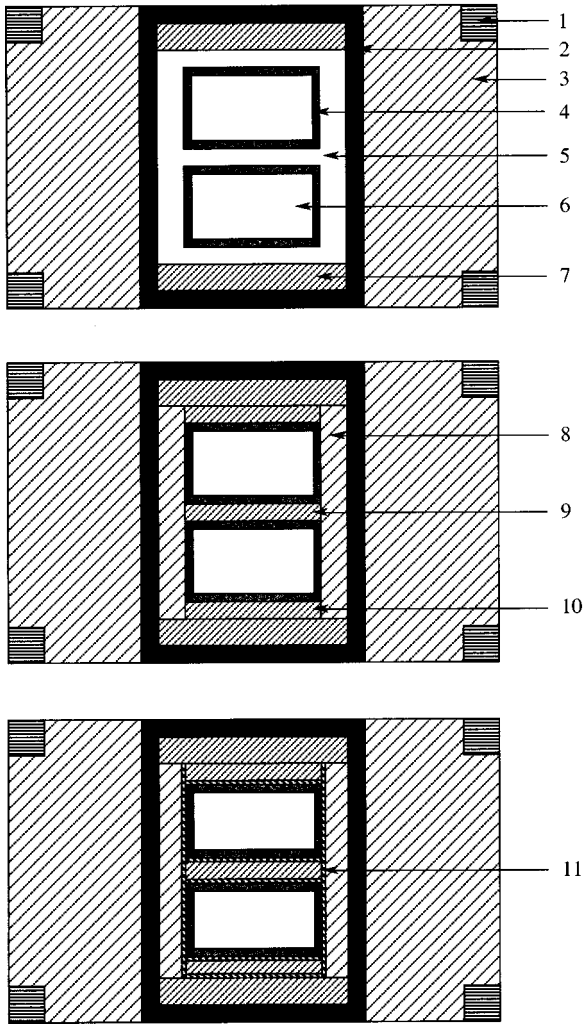

FIG. 2. The cell assemblies for high-pressure synthesis at 1573 K (upper), at 1973 K (middle), and at 2273 K (lower). (1) steel ring, (2) graphite heater, (3) NaCl+10 wt. % ZrO_2, (4) Pt capsule, (5) NaCl, (6) sample, (7) NaCl+20 wt. % ZrO_2, (8) NaCl+10 wt. % ZrO_2, (9) NaCl+20 wt. % ZrO_2, (10) NaCl+20 wt. % ZrO_2, and (11) Ta foil.

KV_6O_{11} was synthesized at 6.0 GPa and at 1573 K using the FB30H press. Successful experiments gave the weight change of the capsule less than 0.4 mg. The typical weight of the capsule including the mixture was 1.2 g. A couple of three-phase regions, KV_6O_{11}-V_2O_3-V_3O_5 and KV_6O_{11}-K_{2-x}-V_8O_{16} (Refs. 32 and 33)-V_2O_4 were observed. Powder x-ray diffraction detected no solid solution in KV_6O_{11}. Trials to obtain ATi_6O_{11} (A=Na, K, Ca, Sr, Ba) compounds failed in this study.

Single crystals of KV_6O_{11} were prepared from stoichiometric mixtures (1) at 6.0 GPa and 1973 K for 60 min

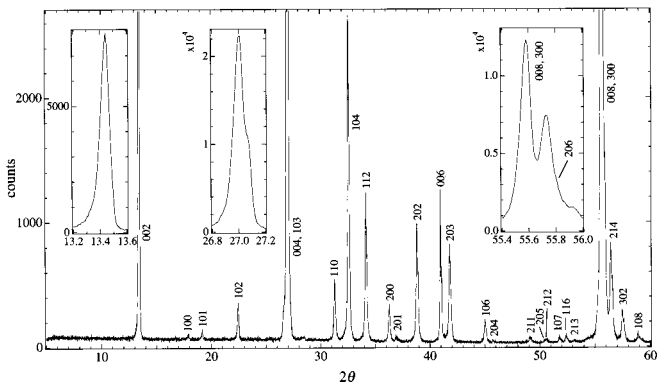

FIG. 3. Powder x-ray diffraction profile of KV_6O_{11} (Cu $K\alpha$). Hexagonal, $P6_3/mmc$, $a=5.7209(5)$ Å, and $c=13.2236(8)$ Å.

(FB30H) for structural analysis, (2) at 5.5 GPa and 2273 K for 30 min, then 1473 K for 30 min (FB30H) for magnetism measurement, and (3) at 5.5 GPa and 2273 K for 120 min (FB40H) for resistivity measurement. The capsules of (1) always showed about 1 mg of weight gain after the synthesis. It was impossible to check the weight change of the capsules of both (2) and (3) because of alloy formation between Pt and Ta. Surfaces of the as-obtained products were slightly oxidized; however, the bulk was not affected.

(1) About 0.2-mm-diam black crystals with hexagonal-plate shape were obtained. Quantitative x-ray microanalysis of the crystals, using $K_2Ti_6O_{13}$ and NaV_6O_{11} as references, determined the K/V ratio of $1/(6.00\pm0.15)$, which supports a composition of KV_6O_{11}. The specimen for diffraction study was cut into 110, 310, and 150 μm parallel to [001], [010], and [210] directions, respectively.

(2) and (3) X-ray microanalysis of the crystals detected no possible impurities such as Pt, Ta, Na, Cl, Zr, or Fe. The single-crystal specimens for the measurements were checked by oscillation and Weissenberg photographs. (2) Obtained crystals were about 0.5 mm in diameter with hexagonal-plate shape. The specimen for the magnetism measurement was 0.07 mg. About 100 crystals were selected and crushed for magnetic susceptibility measurement. (3) Microscopic observation indicated that the product passed through a partially molten state and contained columnar crystals instead of the hexagonal-plate ones. Typical size was 0.1 mm×0.15 mm×0.8 mm. The specimen for the resistivity measurement was 0.15 mm×0.20 mm×1.00 mm. The 0.15 mm×1.00 mm surfaces were perpendicular to [001] direction. The 0.20 mm×1.00 mm surfaces were much more lustrous than the others. About 1.00 mm diameter×0.20 mm thick single crystals may have formed, but broken into pieces during quenching to room temperature or during releasing pressure. Dozens of the crystals were selected and crushed for powder x-ray diffraction (Fig. 3)

B. Structural analysis

Diffraction data for KV_6O_{11} were collected at 295 and 154 K on an Enraf-Nonius CAD4 diffractometer with graphite-monochromatized Mo $K\alpha$ radiation ($\lambda=0.7093$ Å) using ω-θ scan with $\Delta\omega=(0.8+0.35\tan\theta)°$. The measurement at 154 K was carried out by blowing cold nitrogen gas onto the specimen. The temperature was calibrated by a Chromel-Alumel thermocouple with a water-ice standard. Lattice parameters were determined from Bragg angles of 22 reflections in the region $86°<2\theta<89°$ at both temperatures. Reflections for $h\geqslant0$, $k\geqslant0$, $l\geqslant0$, and $|h|\leqslant|k|$ with $2\theta\leqslant90°$ and those for $h\leqslant0$, $k\leqslant0$, $l\leqslant-1$, and $|h|\leqslant|k|$ with $2\theta\leqslant90°$ were measured at both temperatures.

Of the resulting 1280/1272 reflections, 167/45 ones were unobserved (295 K/154 K hereafter in this paragraph). Three standard reflections 600, 240, and 0012 were measured every 4 h. Deviation of intensity was within 0.2%/0.7% during the total exposure time of 84.3 h/123.9 h. No decay correction was applied. An absorption correction[34] was applied with correction factors ($\mu=75.668\,\mathrm{cm}^{-1}$) for F ranging from 1.475/1.477 to 1.764/1.833. 1106/1222 reflections with $I>1.5\sigma(I)$ were used for structural model determination.

Structural parameters including one (single domain model) or two (twin model) scale factor(s) and one free parameter for extinction correction were refined by an anonymous twin refinement program.[35] Atomic scattering factors for neutral atoms and their dispersions were taken from *International Tables for X-ray Crystallography*.[36]

C. Magnetic and electric properties measurement

Magnetic properties were measured using a superconducting quantum interference device (SQUID) magnetometer (Quantum Design, MPMS). Magnetic susceptibility was measured using the crushed specimen (61.87 mg) up to 390 K with external magnetic field of 1000 Oe. The magnetization was studied on the single-crystal specimen (0.07 mg) down to 5 K with an external magnetic field of -5.5×10^4–5.5×10^4 Oe. The resistivity $\rho_\perp$ was measured by a standard four-probe method at 5–246.5 K using a Physical Property Measurement System (Quantum Design). The electrodes were made on the 0.15 mm×1.00 mm surface of the 0.15 mm×0.20 mm×1.00 mm specimen using Au wires (0.033 mm in diameter) and Ag paste (EPO-TEK H20F).

III. RESULTS

A. Structural analysis

At both temperatures, diffraction data showed hexagonal symmetry and an extinction rule, $l\neq$ odd for *hhl*, indicating possible space groups of $P6_3/mmc$, $P\bar{6}2c$, and $P6_3mc$. $P6_3/mmc$ is centrosymmetric and gives a unique structural model. But the other two are not centrosymmetric, and each of the two gives two single-domain models and one twin model. $P\bar{6}2c$ provides a single-domain model [(x,y,z) model], its (110) mirror image [$(-y,-x,z)$ model], and a twin model consisting of the two [$(x,y,z)+(-y,-x,z)$ model]. $P6_3mc$ gives a single-domain model [(x,y,z) model], its (001) mirror image [$(x,y,-z)$ model], and a twin model consisting of the two [$(x,y,z)+(x,y,-z)$ model]. The (x,y,z) and $(-y,-x,z)$ models and the (x,y,z) and $(x,y,-z)$ models are essentially congruent, but differently related to the external form of the specimen. All of the seven models are examined using the same data set for each temperature. To test twin models as well as single-domain models, all of the refinements are carried out on the basis of I instead of F. The results are summarized in Table I.

TABLE I. Structural model examination on KV_6O_{11} at 295 and at 154 K.[a]

T (K)	Space group	Model	N_r	N_p	R (%)	R_w (%)
295	$P6_3/mmc$	unique	1106	26	2.95	4.54
295	$P\bar{6}2c$	(x,y,z)	1106	32	2.91	4.45
295	$P\bar{6}2c$	$(-y,-x,z)$	1106	32	2.91	4.46
295	$P\bar{6}2c$	$(x,y,z)+(-y,-x,z)$	1106	33	2.91	4.44
295	$P6_3mc$	(x,y,z)[b]	1106	43		
295	$P6_3mc$	$(x,y,-z)$[b]	1106	43		
295	$P6_3mc$	$(x,y,z)+(x,y,-z)$[b]	1106	44		
154	$P6_3/mmc$	unique[c]	1222	26	7.07	18.81
154	$P\bar{6}2c$	(x,y,z)[d]	1222	32	6.87	18.49
154	$P\bar{6}2c$	$(-y,-x,z)$[d]	1222	32	6.86	18.48
154	$P\bar{6}2c$	$(x,y,z)+(-y,-x,z)$[d]	1222	33	6.98	18.39
154	$P6_3mc$	(x,y,z)	1222	43	2.80	4.73
154	$P6_3mc$	$(x,y,-z)$	1222	43	2.81	4.77
154	$P6_3mc$	$(x,y,z)+(x,y,-z)$	1222	44	2.70	4.39

[a]To examine twin models as well as single-crystal models, all of the refinements are carried out on the basis of I.
[b]Structural parameters do not converge.
[c]Temperature factors of V(1), V(3), and O(2) are negative.
[d]Temperature factors of V(3), O(1), and O(2) are negative.

1. 295 K

The three $P6_3mc$ models provide low enough R_w values as well as the others. But structural parameters of the three models are oscillating with large amplitudes and do not converge. So the three $P6_3mc$ models are excluded. The three $P\bar{6}2c$ models give slightly smaller R_w values compared to the $P6_3/mmc$ one. Among the four possible models, the $P6_3/mmc$ one provides the highest R_w value of 0.0454 and the $P\bar{6}2c$ twin model the lowest R_w value of 0.0444. However, the difference in R_w for the two models cannot be regarded as significant, taking into account the number of parameters, N_p. Hence the $P6_3/mmc$ model with the highest symmetry is selected for the 295 K structure. A total 1280 of reflections are averaged into 640 unique ones for $P6_3/mmc$ ($R_{\rm int}=0.010$). Here 542 reflections among the 640 ones satisfy the condition $I>1.5\sigma(I)$. The final refinement is carried out on the basis of F using the 542 reflections (Table II).[37] Interatomic distances and bond angles are listed in Table III.

2. 154 K

All of the $P6_3/mmc$ and $P\bar{6}2c$ models result in significantly high R_w values compared to the remaining $P6_3mc$ models. In addition, several temperature factors converge to negative in all of the $P6_3/mmc$ and $P\bar{6}2c$ models. Among the three possible $P6_3mc$ models, the twin model gives the

TABLE II. Atomic coordinates and equivalent thermal parameters (Å^2) in KV_6O_{11} at 295 and 154 K. For both temperatures: $M=520.7407$, hexagonal, $Z=2$, $F(000)=490$, and $B_{\rm eq}=\frac{8}{9}\pi^2(4U_{11}+4U_{22}+3U_{33}-4U_{12})$. 295 K: $P6_3/mmc$, $a=5.7233(1)$ Å, $c=13.2282(2)$ Å, $V=375.25(2)$ Å^3, $d_{\rm calc}=4.609$ g cm^{-3}. Refined on F as a single-crystal specimen, $R=0.016$, $R_w=0.019$, $w=1/\sigma^2(F)$, $\Delta/\sigma<0.006$, and $-1.147<\Delta\rho\leq 0.757$ e Å^3. 154 K: $P6_3mc$, $a=5.7137(2)$ Å, $c=13.1947(3)$ Å, $V=373.05(2)$ Å^3, $d_{\rm calc}=4.636$ g cm^{-3}. Refined on I as a twin specimen, $R=0.026$, $R_w=0.043$, $w=1/\sigma^2(I)$, $\Delta/\sigma<0.006$, and volume fraction (x,y,z): $(x,y,-z)=1.00(6):0.95(6)$.

		295 K ($P6_3/mmc$)						154 K ($P6_3mc$)			
Atom	Position	x	y	z	$B_{\rm eq}$	Atom	Position	x	y	z	$B_{\rm eq}$
K	2c	1/3	2/3	1/4	0.680(7)	K	2b	1/3	2/3	0.252 86(11)	0.359(8)
V(1)	6g	1/2	0	0	0.487(4)	V(1)	6c	0.493 98(2)	2x	0	0.271(3)
V(2)	4e	0	0	0.146 907(18)	0.417(4)	V(21)	2a	0	0	0.147 90(11)	0.249(13)
						V(22)	2a	0	0	0.353 89(10)	0.290(14)
V(3)	2d	1/3	2/3	3/4	0.539(6)	V(3)	2b	1/3	2/3	0.744 62(10)	0.313(8)
O(1)	12k	0.169 30(7)	2x	0.078 91(5)	0.502(8)	O(11)	6c	0.169 55(11)	2x	0.079 88(13)	0.343(18)
						O(12)	6c	0.168 55(10)	2x	0.421 59(12)	0.350(16)
O(2)	6h	0.152 71(10)	2x	3/4	0.544(11)	O(2)	6c	0.152 82(10)	2x	0.749 48(13)	0.392(11)
O(3)	4f	1/3	2/3	0.590 37(9)	0.480(14)	O(31)	2b	1/3	2/3	0.586 89(16)	0.29(2)
						O(32)	2b	1/3	2/3	0.904 63(17)	0.27(3)

TABLE III. Interatomic distances (Å) and bond angles (deg) in KV_6O_{11} at 295 and 154 K. Symmetry codes: (i) x,y,z; (ii) $1-y,\ 1+x-y,\ z$; (iii) $-x+y,\ 1-x,\ z$; (iv) $1-y,\ 1-x,\ 1/2-z$; (v) $-x+y,\ y,\ 1/2-z$; (vi) $x,\ 1+x-y,\ 1/2-z$; (vii) $-x,\ 1-y,\ -1/2+z$; (viii) $1-x,\ 1-y,\ -1/2+z$; (ix) $y,\ -x+y,\ -1/2+z$; (x) $y,\ 1-x+y,\ -1/2+z$; (xi) $x-y,\ x,\ -1/2+z$; (xii) $1+x-y,\ 1+x,\ -1/2+z$; (xiii) $1-y,\ x-y,\ z$; (xiv) $-x+y,\ -x,\ z$; (xv) $y,\ x-z$; (xvi) $1-x,\ -x+y,\ -z$; (xvii) $x,\ x-y,\ 1/2-z$; (xviii) $-y,\ x-y,\ z$, (xix) $-x,\ -y,\ -1/2+z$; (xx) $-x+y,\ y,\ 3/2-z$; (xxi) $1-x+y,\ 1-x,\ z$; (xxii) $x,\ -1+y,\ z$; (xxiii) $1+x-y,\ x,\ -1/2+z$; (xxiv) $x,\ -1+y,\ -1+z$.

295 K ($P6_3/mmc$)		154 K ($P6_3mc$)	
K-O($1^{i,ii,iii,iv,v,vi}$)	2.7868(6)	K-O($11^{i,ii,iii}$)	2.799(2)
		O($12^{i,ii,iii}$)	2.760(2)
O($2^{vii,viii,ix,x,xi,xii}$)	2.8650(1)	O($2^{vii,viii,ix,x,xi,xii}$)	2.8605(1)
V(1)-O($1^{xiii,xiv,xv,xvi}$)	1.9434(4)	V(1^{xxii})-O($11^{xiii,xiv}$)	1.9206(10)
		O($12^{ix,xxiii}$)	1.9655(10)
O($3^{viii,xvii}$)	2.0393(7)	O(31^{viii})	2.0580(12)
		O(32^{xxiv})	2.0276(14)
V(2)-O($1^{i,xiv,xviii}$)	1.9041(6)	V(21)-O($11^{i,xiv,xviii}$)	1.9029(13)
O($2^{ix,xi,xix}$)	2.0375(7)	O($2^{ix,xi,xix}$)	2.0208(16)
		V(22)-O($12^{i,xiv,xviii}$)	1.8922(13)
		O($2^{ix,xi,xix}$)	2.0459(16)
V(3)-O($2^{i,ii,iii}$)	1.7905(9)	V(3)-O($2^{i,ii,iii}$)	1.7876(10)
O($3^{i,xx}$)	2.1116(12)	O(31)	2.081(3)
		O(32)	2.111(2)
V(1)-V(1^{xxi})	2.861 65(5)	V(1^{xxii})-V(1^{xiv})[a]	2.7536(4)
		V(1^{iii})[b]	2.9601(4)
V(2)-V(2^{v})	2.7275(5)	V(21)-V(22)	2.7180(5)
O(1^{xiii})-V(1)-O(1^{xiv})	92.88(4)	O(11^{xiii})-V(1^{xxii})-O(11^{xiv})	93.92(8)
		O(12^{ix})-V(1^{xxii})-O(12^{xxiii})	91.86(7)
O(1^{xiii})-V(1)-O(1^{xvi})	87.13(4)	O(11^{xiii})-V(1^{xxii})-O(12^{xxiii})	87.03(4)
O(1^{xiii})-V(1)-O(3^{viii})	92.00(2)	O(11^{xiii})-V(1^{xxii})-O(31^{viii})	91.79(5)
		O(12^{ix})-V(1^{xxii})-O(32^{xxiv})	91.71(6)
O(1^{xiii})-V(1)-O(3^{xvii})	88.00(2)	O(11^{xiii})-V(1^{xxii})-O(32^{xxiv})	91.28(4)
		O(12^{ix})-V(1^{xxii})-O(31^{viii})	85.16(4)
O(1)-V(2)-O(1^{xiv})	99.51(2)	O(11)-V(21)-O(11^{xiv})	99.57(7)
O(1)-V(2)-O(2^{ix})	89.356(19)	O(11)-V(21)-O(2^{ix})	89.02(3)
O(2^{ix})-V(2)-O(2^{xi})	80.10(3)	O(2^{ix})-V(21)-O(2^{xi})	80.80(8)
		O(12)-V(22)-O(12^{xiv})	99.54(7)
		O(12)-V(22)-O(2^{ix})	89.55(4)
		O(2^{ix})-V(22)-O(2^{xi})	79.61(7)
O(2)-V(3)-O(2^{ii})	120	O(2)-V(3)-O(2^{ii})	119.873(9)
O(2)-V(3)-O(3)	90	O(2)-V(3)-O(31)	92.05(7)
		O(2)-V(3)-O(32)	87.95(7)
V(1)-O(1^{xv})-V(1^{xxi})	94.83(3)	V(1^{xxii})-O(11^{xiii})-V(1^{xiv})[a]	91.59(6)
		V(1^{xxii})-O(12^{ix})-V(1^{iii})[b]	97.70(7)
V(1)-O(3^{viii})-V(1^{xxi})	89.12(4)	V(1^{xxii})-O(32^{xxiv})-V(1^{xiv})[a]	85.54(7)
		V(1^{xxii})-O(31^{viii})-V(1^{iii})[b]	91.97(7)
V(2)-O(2^{ix})-V(2^{v})	84.03(4)	V(21)-O(2^{ix})-V(22)	83.88(4)
V(1)-O(1^{xiv})-V(2)	128.06(2)	V(1^{xxii})-O(11^{xiv})-V(21)	129.65(4)
		V(1^{xxii})-O(12^{ix})-V(22^{ix})	126.63(3)
V(1)-O(3^{viii})-V(3^{viii})	125.89(3)	V(1^{xxii})-O(31^{viii})-V(3^{viii})	123.86(5)
		V(1^{xxii})-O(32^{xxiv})-V(3^{xxiv})	128.36(5)
V(2)-O(2^{ix})-V(3^{viii})	137.986(17)	V(21)-O(2^{ix})-V(3^{viii})	136.40(11)
		V(22)-O(2^{ix})-V(3^{viii})	139.72(11)

[a]Intratrimer.

[b]Intertrimer.

TABLE IV. Electrostatic potentials (φ) and Madelung energies (ΔE) of KV_6O_{11} for possible charge distributions. The V(21) and V(22) atoms are equivalent in the $P6_3/mmc$ form.

	295 K ($P6_3/mmc$)			154 K ($P6_3mc$)		
V(1)	+4	+3.5	+3	+4	+3.5	+3
V(21)	+3	+3.5	+4	+3	+3.5	+4
V(22)	+3	+3.5	+4	+3	+3.5	+4
V(3)	+3	+3.5	+4	+3	+3.5	+4
φ[V(1)](V)	−38.92	−37.50	−36.08	−38.73	−37.31	−35.90
φ[V(21)](V)	−38.56	−41.14	−43.73	−38.71	−41.25	−43.79
φ[V(22)](V)	−38.56	−41.14	−43.73	−38.70	−41.33	−43.96
φ[V(3)](V)	−40.03	−42.04	−44.05	−40.24	−42.26	−44.28
ΔE(MJ mol^{-1})	−5.631	−5.656	−5.727	−5.629	−5.658	−5.733

lowest R_w value. The difference should be significant even if the number of parameters, N_p, is considered. The twin $P6_3\underline{mc}$ model is selected for the 154 K data. A pair of $hk0$ and $\bar{h}k0$ reflections are averaged into an $hk0$ reflection. As a result, a total of 1272 reflections are averaged into 1236 unique ones for $P6_3mc$ ($R_{\rm int}=0.005$). Here 1189 reflections among the 1236 ones satisfy the condition $I>1.5\sigma(I)$. The final refinement was carried out on the basis of I using the 1189 reflections (Table II).[37] Interatomic distances and bond angles are listed in Table III.

Madelung energies are calculated by the Fourier method using an unpublished computer program[38] for both structures at 295 and 154 K. At both temperatures, the V(1) atom prefers the trivalent state and both V(2) and V(3) atoms the tetravalent state (Table IV).

B. Magnetic susceptibility

1. Above T_t

Figure 4 shows χ^{-1} versus temperature of KV_6O_{11}, NaV_6O_{11},[5] and SrV_6O_{11}.[6] The χ^{-1} of KV_6O_{11} shows an anomaly at 190 K ($=T_t$) and is concave upward both above and below T_t. Above T_t, χ^{-1} versus temperature is linear in both NaV_6O_{11} and SrV_6O_{11}, whereas χ^{-1} is concave upward in KV_6O_{11}. The specimen of KV_6O_{11} is obtained by crushing single crystals and is confirmed to be phase pure by powder x-ray diffractometry. The nature of χ in KV_6O_{11} is believed to be intrinsic.

Above T_t, χ data of the three compounds are analyzed, considering that χ consists of the Curie-Weiss paramagnetic term and temperature-independent term as follows:

$$\chi = C/(T-\theta)+\chi_{\rm const}. \quad (1)$$

C and θ represent the Curie constant and Weiss temperature, respectively. $\chi_{\rm const}$ includes the Pauli paramagnetic term (χ_P), Van-Vleck paramagnetic term ($\chi_{\rm VV}$), and Landau diamagnetic term (χ_L). The parameters obtained are shown in Table V. $\chi_{\rm const}$ of NaV_6O_{11} agrees well with that obtained from a Knight shift versus χ plot,[39] 4×10^{-4} emu mol^{-1}. The parameters for SrV_6O_{11} do not converge, probably due to the narrow temperature range of the data. So the analysis is carried out by fixing $\chi_{\rm const}$ of SrV_6O_{11} at $\chi_{\rm const}$ of NaV_6O_{11}, 3.6×10^{-4} emu mol^{-1}. $\chi_{\rm const}$ of KV_6O_{11} converges to 1.89×10^{-3} emu mol^{-1}, which is much larger than that of NaV_6O_{11}. This reflects different curvature in χ^{-1} versus T. However, both KV_6O_{11} and NaV_6O_{11} are metallic and show similar resistivity above T_C. So the two compounds probably show comparable χ_P. The difference, K^+ or Na^+, does not appear to cause so large difference in $\chi_{\rm VV}$ or χ_L. A large $\chi_{\rm const}$ of KV_6O_{11}, 1.89×10^{-3} emu mol^{-1}, may be questionable. χ data of KV_6O_{11} at 190–270 K are reanalyzed by fixing $\chi_{\rm const}$ of KV_6O_{11} at $\chi_{\rm const}$ of NaV_6O_{11} [Table V, spin-free V(1) model]. The Curie constant of KV_6O_{11} obtained in this way is close to that of NaV_6O_{11}. The latter analysis is used for the spin-free V(1) model described later.

2. Below T_t

Below T_t, χ^{-1} versus T is significantly concave upward in KV_6O_{11} as well as in NaV_6O_{11} (Ref. 5) and SrV_6O_{11} (Ref. 6) (Fig. 4). The relationship of χ^{-1} versus T approaches being linear with decreasing temperature. An additional χ term appears to contribute which decreases with decreasing temperature. χ^{-1} versus T is analyzed on the assumption that the additional term is an energy-gap term as follows:

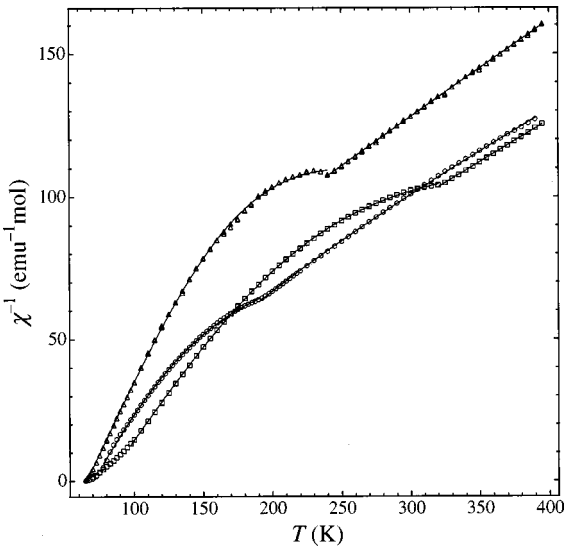

FIG. 4. Inverse magnetic susceptibility vs temperature for KV_6O_{11} (circle), NaV_6O_{11} (Ref. 5) (triangle), and SrV_6O_{11} (Ref. 6) (square). The fitting curve above T_t for KV_6O_{11} is on the basis of the spin-gap V(1) model (see text). Those for both NaV_6O_{11} and SrV_6O_{11} are on the basis of the spin-free V(1) model. The fitting curves below T_t for the three compounds are on the basis of Eq. (2) (see text).

TABLE V. Parameters characterizing the paramagnetic states of AV_6O_{11} compounds.

	KV_6O_{11}	NaV_6O_{11}	SrV_6O_{11}
$T \leqslant T_t$			
C (emu K mol^{-1})	1.20(3)	0.968(5)	1.431(5)
$p_{\mathrm{eff}}(n=3)$	1.79	1.61	1.95
$p_{\mathrm{eff}}(n=2)$	2.19	1.97	2.39
$p_{\mathrm{eff}}(n=1)$	3.10	2.78	3.38
θ (K)	70.1(4)	65.57(13)	79.20(15)
A (emu mol^{-1})	0.0148(18)	0.0255(15)	0.0144(3)
Δ (K)	200(28)	494(15)	472(8)
χ_{const} (emu mol^{-1})	3.6×10^{-4}	3.6×10^{-4}	3.6×10^{-4}
$T_t \leqslant T$ [spin-free V(1) model]			
C (emu K mol^{-1})	2.733(7)	2.670(11)	3.142(14)
$p_{\mathrm{eff}}(n=3)$	2.70	2.67	2.89
$p_{\mathrm{eff}}(n=2)$	3.30	3.27	3.54
$p_{\mathrm{eff}}(n=1)$	4.67	4.62	5.01
θ (K)	12.5(5)	$-58(7)$	$-17.1(17)$
χ_{const} (emu mol^{-1})	3.6×10^{-4}	$3.6(14)\times10^{-4}$	3.6×10^{-4}
$T_t \leqslant T$ [spin gap V(1) model]			
C_1 (emu K mol^{-1})	2.301(18)	2.99(7)	2.68(9)
$p_{\mathrm{eff}}(n=3)$	2.48	2.82	2.67
θ_1 (K)	$-236(4)$	$-608(24)$	$-469(28)$

$$\chi = C/(T-\theta) + A\exp(-\Delta/T) + \chi_{\mathrm{const}}. \quad (2)$$

A is a constant and Δ corresponds to the energy gap. The gap term has been applied for $Ni(C_2H_8N_2)_2NO_2(ClO_4)$,[40] a typical Haldane gap[41] system. Equation (2) fits well the data (Fig. 4). Analyses are performed by fixing χ_{const} at 3.6×10^{-4} emu mol^{-1} (Table V). Other forms such as $AT^{-1/2}\exp(-\Delta/T)$ and $AT^{-1}\exp(-\Delta/T)$ are tried as well. The former[42] has been applied for two-leg spin ladder systems, $SrCu_2O_3$ (Ref. 43) and CaV_2O_5.[44] The latter has been applied for the spin gap in $CaCuGe_2O_6$.[45] However, quality of the fitting is essentially independent of the form of the gap term. The parameters A and Δ vary significantly depending on the form, but the parameters C and θ are almost independent of the form. So the simplest form $A\exp(-\Delta/T)$ is adopted.

C. Magnetization

KV_6O_{11} shows uniaxial magnetic anisotropy with an easy axis of magnetization parallel to [001] at 5 K [Fig. 5(a)]. KV_6O_{11} behaves as a magnetically single domain with a coercive force of 1.8×10^3 Oe at 5 K [Fig. 5(b)]. The hysteresis at zero field survives below 40 K but above 45 K. Figure 6 shows the initial magnetization curves of KV_6O_{11} with magnetic field parallel to [001]. At 5 K, the magnetization saturates at about 850 Oe, which may correspond to the demagnetizing field. The demagnetizing field is not corrected throughout this work. Even above saturation, the magnetization increases gradually with increasing magnetic field. The magnetization curves above saturation can be regarded as linear lines below 50 K, but the curves are concave upward above 55 K. The slopes of the linear lines, χ_{hf}, are plotted against temperature in Fig. 7. χ_{hf} increases linearly with increasing temperature as follows:

$$\chi_{\mathrm{hf}} = pT + q. \quad (3)$$

However, the slope p is smaller below 35 K [$p = 0.065(3)$ emu mol^{-1} K^{-2}, $q = 4.66(6)$ emu mol^{-1} K^{-1}] and larger above 35 K [$p = 0.321(8)$ emu mol^{-1} K^{-2}, $q = -4.3(4)$ emu mol^{-1} K^{-1}]. The two fitting lines in Fig. 7 intersect each other at 35.2 K.

The initial magnetization curves (Fig. 6) are analyzed by means of an M^2 versus H/M plot, $M^{5/2}$ versus $(H/M)^{3/4}$ plot,[5,46] and M^4 versus H/M one[47] (Fig. 8). The first one has been derived from the mean field theory and is well known as the Arrot plot. The second one is relatively empirical and has been applied for Ni (Ref. 46) and NaV_6O_{11}.[5] The third one has been derived from the self-consistent renormalization (SCR) theory[48] and has been applied for the weakly itinerant ferromagnetism of $Fe_{0.83}Co_{0.17}Si$.[49] Arrott plots are concave upward at 55–75 K [Fig. 8(a)]. $M^{5/2}$ versus $(H/M)^{3/4}$ plots are slightly concave downward below 60 K, but linear above 62 K. Their slopes increase with increasing temperature. M^4 versus H/M plots are slightly concave downward below 25 K, linear at 30–64 K, and concave downward again above 65 K. Their change in slope with respect to temperature is much milder than that of $M^{5/2}$ versus $(H/M)^{3/4}$ plots. In any case, at least above T_C, successful plots are expected to be linear with a constant slope independent of temperature. As the $M^{5/2}$ versus $(H/M)^{3/4}$ plots show the best linearity around T_C, T_C is determined by the relationship of $M^{5/2}$ intercept versus temperature. The T_C obtained is 66.8 K. The saturated magnetization M_s at each temperature is analyzed by three methods: (1) from the magnetization curves above saturation, regarding as linear below 50 K and parabolic at 55–62 K, (2) from the $M^{5/2}$ intercepts of the $M^{5/2}$ versus $(H/M)^{3/4}$ plots at 5–66 K, and (3) from the M^4 intercepts of the M^4 versus H/M plots at 5–64 K. The M_s values obtained by the three methods show insignifi-

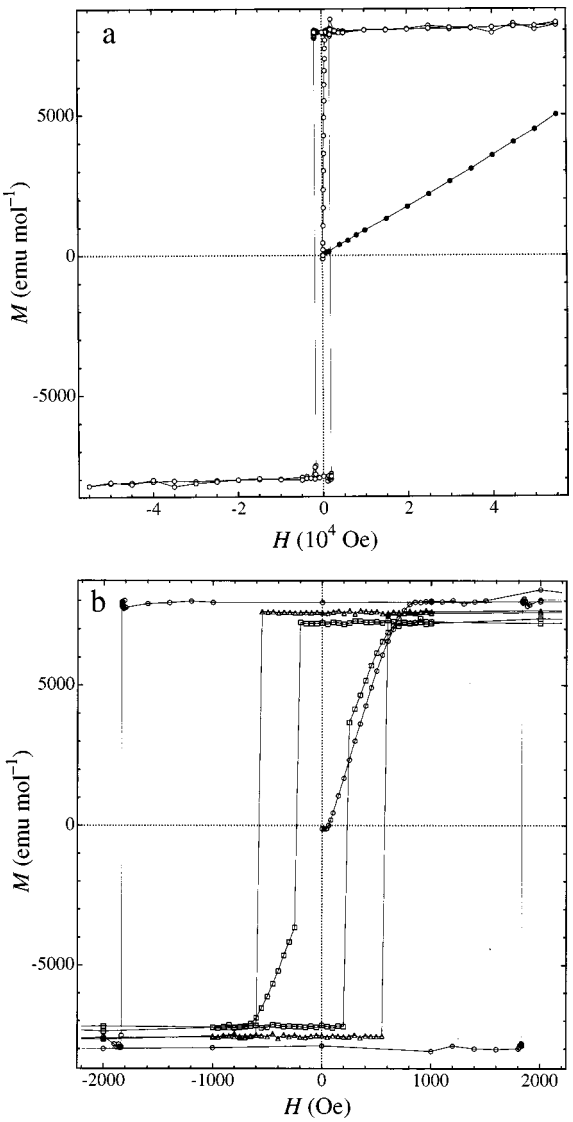

FIG. 5. Hysteresis loops of KV_6O_{11} with external magnetic field parallel to the [001] direction (open shapes) and initial magnetization curve of KV_6O_{11} with magnetic fields perpendicular to [001] (solid circle). (a) whole, 5 K and (b) magnified, 5 K (circle), 30 K (triangle), and 40 K (square).

cant differences. In what follows, M_s values given by (2) will be adopted (Fig. 9). The M_s values of NaV_6O_{11} are obtained by (1) below 53 K and by (2) above 55 K (Fig. 9).[5] By an extrapolation described later, the saturated magnetization at 0 K, $M_s(0\,\mathrm{K})$, of KV_6O_{11} is determined to be $1.5\,\mu_B$ f.u.$^{-1}$. $M_s(0\,\mathrm{K})$ of NaV_6O_{11} (Ref. 5) is $1.7\,\mu_B$ f.u.$^{-1}$.

D. Resistivity

Resistivity of KV_6O_{11} is measured perpendicular to the [001] direction at 5–246.5 K (Fig. 10). Reproducible data are not obtained above 246.5 K in this study. $\rho_\perp$ is of the order of $10^{-4}\,\Omega$ cm. $\rho_\perp$ shows anomalies at 190, 66.5, and 35.1 K which correspond to T_t, T_C, and the anomaly in χ_{hf}, respectively. $\partial\rho_\perp/\partial T$ is positive below 66.5 K and above 190 K, and is concave upward at 66.5–190 K, showing a broad maximum at around 90 K. $\rho_\perp$ exhibits Fermi-liquid-type behavior below 35.1 K, and $\rho_\perp$ versus T is linear between 35.1 and 66.5 K as follows. The transition temperature 35.1 K agrees well with corresponding 35.2 K in χ_{hf}. In what follows, 35.1 K will be adopted as the transition temperature:

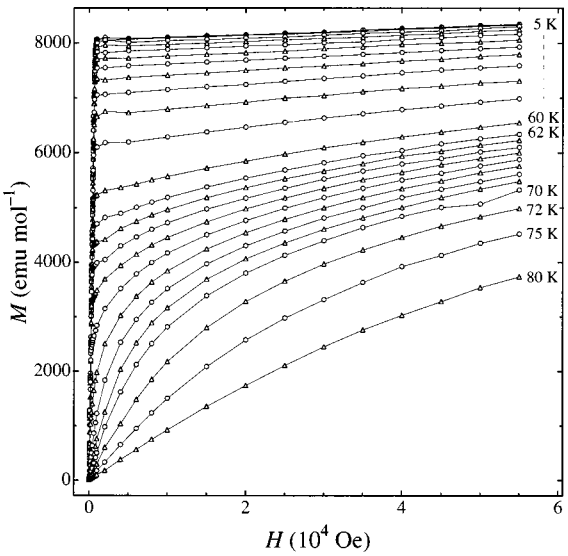

FIG. 6. Initial magnetization curves of KV_6O_{11} with a magnetic field parallel to [001]. 5–60 K: every 5 K. 62–70 K: every 1 K.

$$\rho_\perp = 1.869(7)\times10^{-7}T^2 + 1.604(4)\times10^{-4}\ [\Omega\,\mathrm{cm}] \quad (\text{at } 5\text{–}35.1\ \mathrm{K}), \tag{4}$$

$$\rho_\perp = 6.197(18)\times10^{-6}T + 1.732(9)\times10^{-4}\ [\Omega\,\mathrm{cm}] \quad (\text{at } 35.1\text{–}66.5\ \mathrm{K}). \tag{5}$$

IV. DISCUSSION

A. Crystal structure

Twelve-coordinated K^+ (ionic radius=1.64 Å) is much larger than corresponding Na^+ (1.39 Å), Sr^{2+} (1.44 Å), and Pb^{2+} (1.49 Å).[50] However, the differences between the K-O distances in KV_6O_{11} and the corresponding A-O distances in

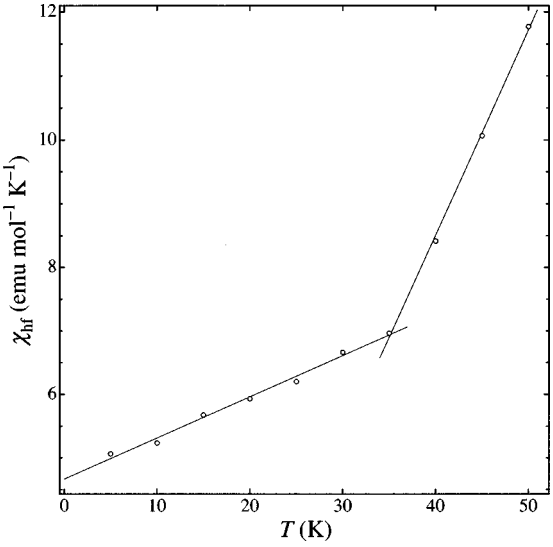

FIG. 7. χ_{hf} vs temperature for KV_6O_{11}.

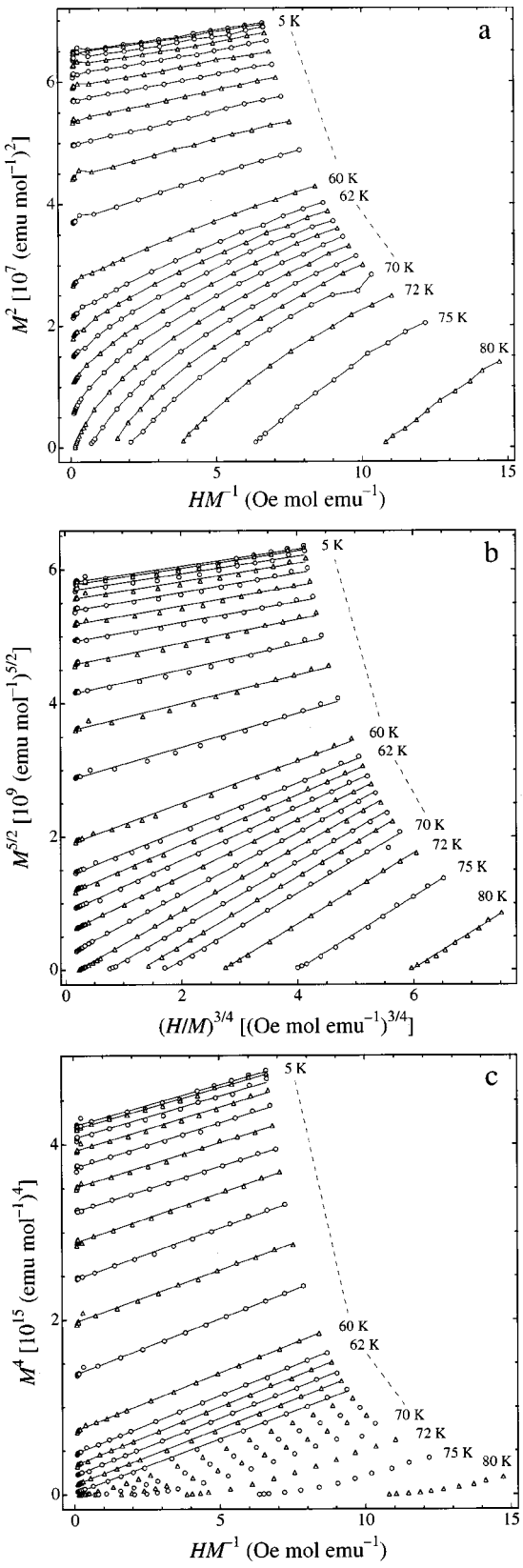

FIG. 8. Isothermal (a) M^2 vs H/M plots, (b) $M^{5/2}$ vs $(H/M)^{3/4}$ plots, and (c) M^4 vs H/M plots for KV_6O_{11}.

AV_6O_{11} (A=Na, Sr, Pb) are much smaller than those expected. The cation should be as large as four-coordinated O^{2-} (1.38 Å) (Ref. 50) to form hexagonal close-packed layers. The pressure of 5.5–6.0 GPa appears to be effective to shrink K^+ with respect to O^{2-} to form the hexagonal close-packed layers.

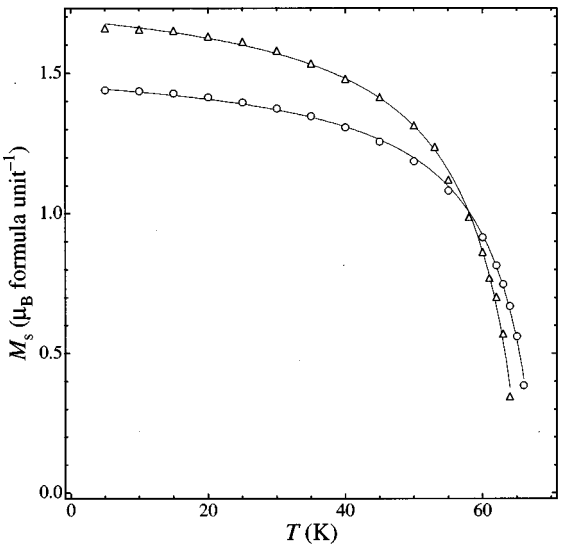

FIG. 9. M_s vs temperature of KV_6O_{11} (circle) and NaV_6O_{11} (Ref. 5) (triangle). The fitting curves are on the basis of Eq. (7) (see text).

The $P6_3mc$ phase of KV_6O_{11} shows twinning (Table I), which suggests that corresponding twinning may occur in NaV_6O_{11} and/or PbV_6O_{11}. However, the structural refinements on the $P6_3mc$ forms of NaV_6O_{11} (Ref. 8) and PbV_6O_{11} (Ref. 3) converged promptly with low enough R factors, without applying twinning. This may be attributable to small anomalous dispersion terms of Na in NaV_6O_{11} or may suggest that the volume fraction ratio $(x,y,z)/(x,y,-z)$ is far from 1.0 in PbV_6O_{11} and/or in NaV_6O_{11}. In the $P6_3mc$ state of KV_6O_{11}, the differences in the atomic coordinates are insignificant between the twin model and the single-domain models. The twin $P6_3mc$ model should be examined in both NaV_6O_{11} and PbV_6O_{11}, even though we cannot expect so much improvement.

KV_6O_{11} shows a $P6_3/mmc$-$P6_3mc$ second-order structural phase transition at a temperature between 154 and 295

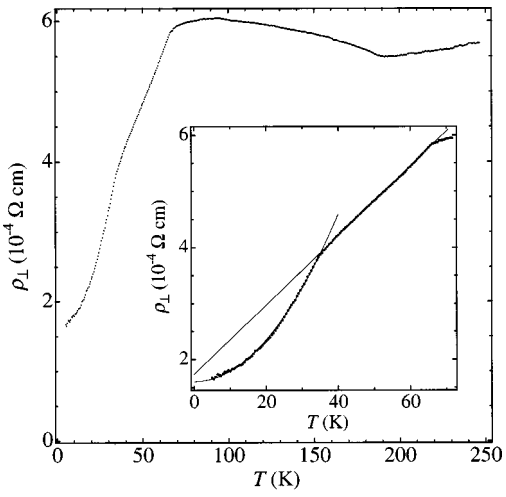

FIG. 10. Resistivity of KV_6O_{11} perpendicular to [001] as a function of temperature.

K (Tables I and II) as NaV_6O_{11} (Refs. 8 and 15) does. Both χ^{-1} and $\rho_\perp$ of KV_6O_{11} show anomalies at 190 K, without any other break point between 154 and 295 K (χ^{-1}) or between 154 and 246.5 K ($\rho_\perp$) (Figs. 4 and 10). Considering the case in NaV_6O_{11},[4,5,8,15] the structural transition in KV_6O_{11} is expected to occur at 190 K. Though the transition temperature should be confirmed, for example, by specific heat, the discussion will be continued assuming that the $P6_3/mmc$-$P6_3mc$ transition accompanies the anomalies in both $\rho_\perp$ and χ^{-1} at $T_t = 190$ K.

The $V(1)O_6$ and $V(2)O_6$ octahedra in KV_6O_{11} are quite similar to the corresponding octahedra in NaV_6O_{11},[7,8] especially in the $P6_3/mmc$ state. The $V(3)O_5$ trigonal bipyramid in KV_6O_{11} shows, however, a small difference compared to that in NaV_6O_{11}. The distance between V(3) and axial O(3) in KV_6O_{11} is longer than that in NaV_6O_{11}.

Among AV_6O_{11} compounds (A=K, Na, Sr, Pb), T_t shows drastic difference [K, 190 K; Na, 240 K;[5] Sr, 320 K;[6] Pb, 560 K (Ref. 28)] but T_C does not show so much difference [K, 66.8 K; Na, 64.2 K;[5] Sr, 70 K;[6] Pb, 90 K (Refs. 13 and 28)]. In NaV_6O_{11}, the transition at T_t accompanies the $P6_3/mmc$-$P6_3mc$ transition, but the transition at T_C does not accompany any structural transition.[15] The magnetic transition at T_t appears to be strongly correlated with the $P6_3/mmc$-$P6_3mc$ structural transition, namely, the V(1) *kagomé* trimer formation, the V(2) branching, or the distortion of the $V(3)O_5$ polyhedra from trigonal bipyramid toward tetrahedron, whereas the magnetic ordering formation at T_C appears to be insensitive to the structural features.

The charge distribution among the V cations in KV_6O_{11} may obey electrostatic stability, though KV_6O_{11} is fundamentally metallic (Fig. 10). Madelung energy calculations suggest that the V(1) sites prefer trivalent cations and the V(2) tetravalent cations in both $P6_3/mmc$ and $P6_3mc$ forms of KV_6O_{11} (Table IV), NaV_6O_{11},[7] and SrV_6O_{11}.[7,27] The V(3) sites prefer tetravalent cations in KV_6O_{11} and NaV_6O_{11},[7] whereas the trivalent one in SrV_6O_{11}.[7,27] The $P6_3mc$ form of PbV_6O_{11} shows a different preference[3] probably due to large structural distortion caused by the steric hindrance of the electron lone pair of Pb^{2+}. The $V(1)O_6$ octahedra of the AV_6O_{11} compounds (A=K, Na, Sr, Pb) forming a *kagomé* lattice show similar Jahn-Teller distortion: apical V(1)-O(3) distances are longer than basal V(1)-O(1) distances. The O(3) atom caps the $V(3)O(2)_3$ triangle to form a $V(3)O(2)_3O(3)_2$ coordination trigonal bipyramid. The distortion is observed in both $P6_3/mmc$ and $P6_3mc$ forms. The t_{2g} states of the V(1) atom separate into two types, higher (d_{xy}) and lower (d_{xz} and d_{yz}), where the z direction corresponds to the apical axis. So d electrons in the V(1) atom are considered to occupy the d_{xz} and/or d_{yz} orbitals (Fig. 11). Similar orbital ordering has been discussed on NaV_6O_{11} (Refs. 8 and 12) and on the ordered rock salt-type insulator $LiVO_2$.[51] The trimer formation in ordered rocksalt type results in a super structure formation,[51] whereas the trimer formation in the *kagomé* lattice does not (Fig. 11). This is consistent with the $P6_3mc$ forms of NaV_6O_{11} (Ref. 8) and KV_6O_{11}.

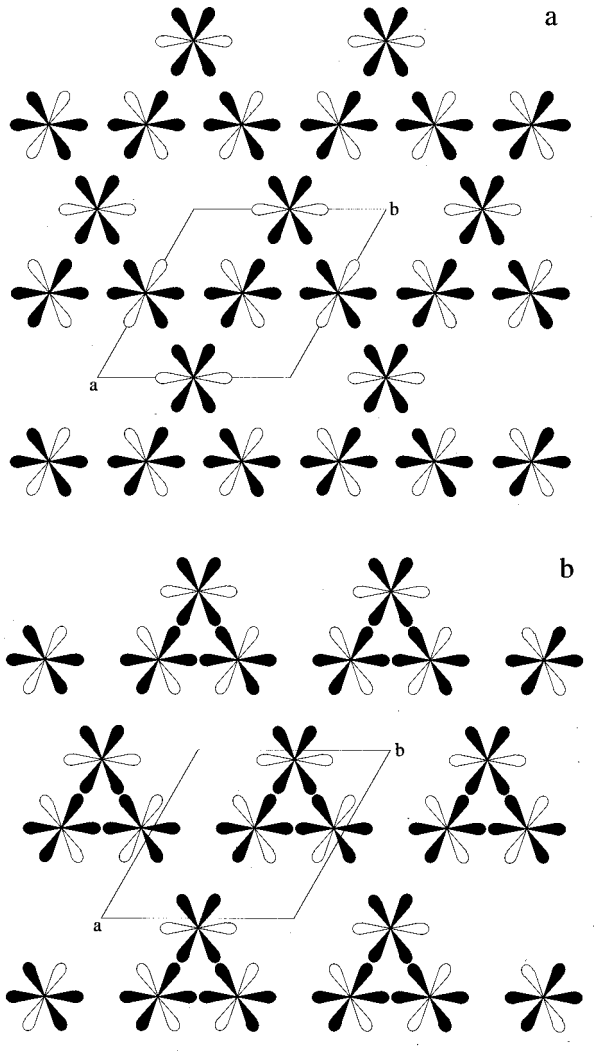

FIG. 11. Schematic view of t_{2g} orbitals of the V(1) *kagomé* lattice in (a) $P6_3/mmc$ form and (b) $P6_3mc$ form. Only in-plane lobes are drawn. The solid and open lobes show occupied and unoccupied orbitals, respectively.

B. Paramagnetic states

1. Spin gap V(1) model

The V(1) atoms from a *kagomé* trimer below T_t and the V(1)-V(1) distance branches into the longer and the shorter ones. The V(2) atoms branch into two types below T_t; however, the V(2)-V(2) distance is maintained almost constant, independent of the transition at T_t. the V(3) coordination polyhedron shows distortion below T_t; however, the V(3) atoms is apparently distant from any adjacent V atom compared to the V(1) and V(2) atoms. So the energy gap term of χ below T_t may be attributable to the V(1) atom. Then the V(2) and/or V(3) atoms are responsible for the Curie-Weiss term below T_t. Provided that that V(2) and/or V(3) atoms maintain their magnetic character above T_t also, the Curie-Weiss term above T_t should consist of two terms, the V(1) term and the V(2)+V(3) term as follows:

$$\chi = C_1/(T-\theta_1) + C_{2,3}/(T-\theta_{2,3}) + \chi_{\text{const}}. \qquad (6)$$

$C_1/(T-\theta_1)$ corresponds to the V(1) atom and $C_{2,3}/(T-\theta_{2,3})$ corresponds to the V(2) and V(3) atoms. Analyses are carried out by fixing $C_{2,3}$, $\theta_{2,3}$, and χ_{const} to C, θ, and χ_{const} below T_t (Fig. 4). The C_1 and θ_1 obtained (Table V) appear to be reasonable.

The model gives the following conclusions. The V(1) atom shows Curie-Weiss character above T_t, whereas spin-

gap character below T_t. The spin moment of the V(1) atom above T_t corresponds to $S=1$ in NaV_6O_{11} and to slightly smaller than $S=1$ in both KV_6O_{11} and SrV_6O_{11}. The V(2) and V(3) atoms show Curie-Weiss character throughout the paramagnetic state. Their Curie constant and Weiss temperature are unchanged by the transition at T_t. Provided that the V(2) and V(3) atoms uniformly contribute to the Curie-Weiss term, their spin moments correspond to almost $S=1/2$ in both KV_6O_{11} and NaV_6O_{11} and to slightly larger than $S=1/2$ in SrV_6O_{11}. Thus the given charge distributions are consistent with electrostatic stability. The Weiss temperature θ_1 and the gap temperature Δ of the V(1) atom show comparable absolute values in the three compounds, which would be reasonable. Positive $\partial\rho_\perp/\partial T$ above T_t and negative $\partial\rho_\perp/\partial T$ below T_t are consistent with this model.

The V(1)-V(1) distance in the $P6_3/mmc$ form is short enough to consider a t_{2g}-t_{2g} hybridization in the V(1) *kagomé* lattice (Table III). Combined with earlier discussions, each d_{xz} and d_{yz} orbital of the V(1) atom is expected to contain nearly one electron (Fig. 11). The two orbitals d_{xz} and d_{yz} are degenerate above T_t. Below T_t, the degeneracy fails and the two orbitals branch into two types, bonding and antibonding. This feature is consistent with spin-gap character below T_t. The gap temperature may be controlled by competition between the energy gap of the bonding and antibonding states and the Coulomb repulsion among the d electrons.

2. Spin-free V(1) model

The above model is, however, in conflict with the NMR study that the V(1) atom of NaV_6O_{11} exhibits negligible spin moment throughout the paramagnetic states.[39] Two ^{51}V NMR absorption peaks of NaV_6O_{11} are detected at 300 K.[6] One exhibits a small Knight shift of -0.1% and the shift is almost independent of temperature. The Knight shift of the other is -2% at 300 K, and the negative shift increases on cooling. The latter peak split into two in the $P6_3mc$ state. Recently, the former was assigned to the V(1) atom and the latter peaks to the V(2) and V(3) atoms.[39] It means that the V(1) atom shows almost negligible spin moment throughout the paramagnetic region and that the temperature dependence of χ is almost exclusively caused by the V(2) and V(3) atoms. In what follows, the discussion will be continued, considering that the temperature-dependent terms of KV_6O_{11} and SrV_6O_{11} are also attributable exclusively to the V(2) and/or V(3) atoms.

Effective Bohr magneton numbers $p_{\rm eff}$ are calculated assuming that one ($n=1$), two ($n=2$), or three ($n=3$) of the V(2) and V(3) atoms per unit formula uniformly contribute the Curie-Weiss term (Table V). In all of the compounds above T_t, both models with $n=1$ and 2 are excluded because the $p_{\rm eff}$ values significantly exceed the theoretical value for $S=1$ (V^{3+}), 2.828. The $p_{\rm eff}$ values with $n=3$ are consistent with $S=1$, especially in SrV_6O_{11}. In the three compounds above T_t, consequently, both V(2) and V(3) atoms are close to trivalent with $S=1$. The V(1) atoms are close to 4+ in both KV_6O_{11} and NaV_6O_{11} and to 3.67+ in SrV_6O_{11}. The charge distribution does not obey the electrostatic stability mentioned earlier. However, the distribution is consistent with the fact that the cation of a face-sharing coordination octahedron prefers lower valence to the cation of an edge-sharing one. In the three compounds, d electrons of the V(1) atoms are considered to be band type and to exhibit negligible spin. The V(1) layer with band electrons and the V(2) and V(3) layer with localized electrons stack alternatively parallel to [001]. This model, however, cannot explain why $\rho_\parallel$ is much lower than $\rho_\perp$ in NaV_6O_{11}.

Mean V-O distance for the V(1), V(2), and V(3) atoms are almost constant between 295 K (above T_t) and 154 K (below T_t) in KV_6O_{11}. This is also observed in both NaV_6O_{11} (Refs. 7 and 8) and SrV_6O_{11}.[7,27] The transitions at T_t probably do not cause charge transfer among the V atoms, if any, to be negligible. At the transitions, the V(1) atoms are considered to maintain their valences and the band character with negligible spin in the three compounds, whereas the V(2) and V(3) atoms change their character below I_t. Provided that all of the V(2) and V(3) atoms uniformly contribute to the Curie-Weiss term below T_t as well, their $p_{\rm eff}$ values almost correspond to $S=1/2$ in the three compounds. Remaining electron spins are considered to decrease with decreasing temperature, obeying $A\exp(-\Delta/T)$. So the V(2) and V(3) atoms include both Curie-Weiss type and spin-gap-type spins below T_t, which would be questionable. In addition, this model cannot explain why $\rho_\parallel$ does not show any anomaly at T_t in spite of the fact that $\rho_\perp$ shows an anomaly at T_t in NaV_6O_{11}.

C. Below T_C

Arrot plots of both KV_6O_{11} and NaV_6O_{11} are not linear at all [Fig. 8(a)], which suggests that well-known mean field theory is not applicable to their magnetization. Their temperature dependence of $\rho_\perp$ resembles those of well-known magnetic metals such as Fe.[52] $M_s(0\,{\rm K})$ of neither KV_6O_{11} nor NaV_6O_{11} is integer (Fig. 9). Their M_s values at 5 K increase with increasing H even above saturation. M^4 versus H/M plots show much better linearity than the Arrot plots in KV_6O_{11}. These features suggest itinerant ferromagnetism.

Both plots, M_s^2 versus $T^{4/3}$ and M_s^2 versus T^2 (Fig. 12), are not linear, which suggests that the origin of the magnetization is not spin fluctuations.[47,49] M_s versus temperature of both KV_6O_{11} and NaV_6O_{11} can be analyzed by a hyperbolic function, like Curie-Weiss paramagnetism, as follows:

$$M_s = C'/(T-\theta') + M_{\rm const}. \tag{7}$$

Though Eq. (7) has no theoretical background so far, it fits all of the data (Fig. 9). The parameters obtained are $C'=8.8(4)\mu_B\,{\rm f.u.}^{-1}\,{\rm K}$, $\theta'=73.6(3)$ K, and $M_{\rm const}=1.572(9)\mu_B\,{\rm f.u.}^{-1}$ for KV_6O_{11} and $C'=12.0(6)\mu_B\,{\rm f.u.}^{-1}\,{\rm K}$, $\theta'=72.1(4)$ K, and $M_{\rm const}=1.854(15)\mu_B\,{\rm f.u.}^{-1}$ for NaV_6O_{11}. M_s at 0 K and T_C are given by extrapolating the plot to $T=0$ K and $M_s=0\,\mu_B\,{\rm f.u.}^{-1}$, respectively. Thus obtained parameters are $M_s(0\,{\rm K})=1.5\mu_B\,{\rm f.u.}^{-1}$ and $T_C=68$ K for KV_6O_{11} and $M_s(0\,{\rm K})=1.7\mu_B\,{\rm f.u.}^{-1}$ and $T_C=66$ K for NaV_6O_{11}. The T_C values are slightly higher than those obtained by the relationship $M^{5/2}$ intercept versus temperature described earlier; however, the $M_s(0\,{\rm K})$ values are reasonable.

KV_6O_{11} and NaV_6O_{11} show a similar temperature dependence of $\rho_\perp$. Both compounds show three discontinuities in

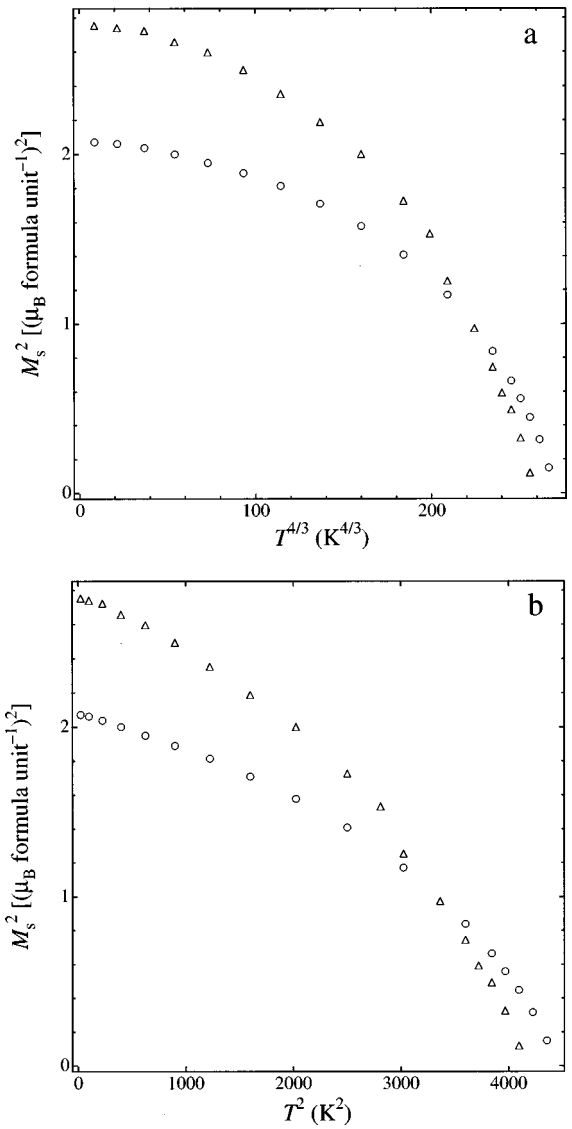

FIG. 12. (a) M_s^2 vs $T^{4/3}$ plots and (b) M_s^2 vs T^2 plots for KV_6O_{11} (circle) and NaV_6O_{11} (Ref. 5) (triangle).

$\partial\rho_\perp/\partial T$. Those at T_C and T_t are common, but the remaining one is different. NaV_6O_{11} (Ref. 5) shows the remaining one (80 K) in the paramagnetic state between T_C and T_t. The discontinuity accompanies a structural transition, but no anomaly in χ, whereas in KV_6O_{11}, the remaining discontinuity (35.1 K) is observed below T_C (Fig. 10). In addition, the discontinuity accompanies an anomaly in $\partial\chi_{hf}/\partial T$ (Fig. 7). In itinerant ferromagnetic system, χ_{hf} is sensitive to the band structure and/or the difference between the density of states for up spin and down spin. So the magnetic structure, the band structure, and/or the difference in the density of states of KV_6O_{11} may change at 35.1 K. A structural transition may also occur at 35.1 K.

Below T_C, $\rho_\perp$ versus T of NaV_6O_{11} is linear down to about 30 K and becomes concave downward. The change in the slope is continuous. The corresponding $\rho_\perp$ versus T of KV_6O_{11} is also linear down to 35.1 K. However, the relationship changes into parabolic below 35.1 K, indicating Fermi liquid character (Fig. 10).

V. CONCLUSION

An AV_6O_{11}-type magnetic metal KV_6O_{11} was discovered by a high-pressure synthesis at 5.5–6.0 GPa. It crystallizes in hexagonal $P6_3/mmc$ at 295 K, whereas in hexagonal $P6_3mc$ at 154 K. KV_6O_{11} shows three magnetic transitions at 190 K ($=T_t$), 66.8 K ($=T_C$), and 35.1 K. The paramagnetic states were analyzed on the basis of the spin-gap V(1) model and spin-free V(1) model. (1) Spin-gap V(1) model: The V(1) atom shows Curie-Weiss character with $S=1$ above T_t, but exhibits spin-gap character below T_t. The V(2) and V(3) atoms show Curie-Weiss character corresponding to $S=1/2$ throughout the paramagnetic states. (2) Spin-free V(1) model: The V(1) atom is almost tetravalent and free from electron spin throughout the paramagnetic states. The V(2) and V(3) atoms show Curie-Weiss character with $S=1$ above T_t, whereas below T_t, half of the spin survives as Curie-Weiss type, but the remaining half exhibits spin-gap character. Both models have several problems. KV_6O_{11} shows uniaxial magnetic anisotropy with an easy axis of magnetization parallel to the [001] direction below T_C. The saturated magnetization versus temperature cannot be explained by the well-known mean field theory or spin fluctuation mechanism, but exhibits a hyperbolic relationship. KV_6O_{11} is essentially metallic. The resistivity normal to [001], $\rho_\perp$, is of the order of $10^{-4}\,\Omega\,\mathrm{cm}^{-1}$. $\rho_\perp$ versus T shows a positive slope above 190 K, a broad maximum at around 90 K, a linear relationship with positive slope between 35.1 and 66.8 K, and Fermi-liquid-type behavior below 35.1 K. Specific heat studies are required especially to understand the Fermi liquid state below 35.1 K. Neutron and NMR studies are required especially to reveal the origin of the unusual paramagnetism below T_t and the magnetic structure (s) below T_C.

ACKNOWLEDGMENTS

The author is grateful to M. Akaishi (NIRIM) and T. Kawashima (NIRIM) for significant support on high-pressure experiments, E. Takayama-Muromachi (NIRIM) for encouraging high-pressure synthesis and valuable discussions of magnetic susceptibility, K. Kato (NIRIM) for valuable advice on structural analysis, and H. Kato (Kyoto University) for kindly allowing the author to quote unpublished data on PbV_6O_{11}. The author is indebted to H. Tsunetsugu (University of Tsukuba), M. Umehara (NIRIM), Y. Uchida (NIRIM), E. Kita (University of Tsukuba), M. Arai (NIRIM), and Y. Takahashi (Himeji Institute of Technology) for valuable discussions of magnetism. The author is grateful to A. Sato (NIRIM) for help on the diffraction experiment and K. Kosuda (NIRIM) for x-ray microanalysis. This work was supported by the Science and Technology Agency of Japan.

[1] M. E. de Roy, J. P. Besse, R. Chevalier, and M. Gasperin, J. Solid State Chem. **67**, 185 (1987).
[2] Y. Kanke, F. Izumi, E. Takayama-Muromachi, K. Kato, T. Kamiyama, and H. Asano, J. Solid State Chem. **92**, 261 (1991).
[3] O. Mentre and F. Abraham, J. Solid State Chem. **125**, 91 (1996).
[4] Y. Kanke, E. Takayama-Muromachi, K. Kato, and Y. Matsui, J. Solid State Chem. **89**, 130 (1990).
[5] Y. Uchida, Y. Kanke, E. Takayama-Muromachi, and K. Kato, J. Phys. Soc. Jpn. **60**, 2530 (1991).
[6] Y. Uchida, Y. Kanke, and Y. Onoda, in *Ferrites*, Proceedings of the Sixth International Conference on Ferrites (ICF6), Tokyo, 1992 (Japan Society of Powder and Powder Metallurgy, Tokyo, 1992).
[7] Y. Kanke, K. Kato, E. Takayama-Muromachi, and M. Isobe, Acta Crystallogr., Sect. C: Cryst. Struct. Commun. **48**, 1376 (1992).
[8] Y. Kanke, F. Izumi, Y. Morii, E. Akiba, S. Funahashi, K. Kato, M. Isobe, E. Takayama-Muromachi, and Y. Uchida, J. Solid State Chem. **112**, 429 (1994).
[9] Y. Kanke, H. Shigematsu, K. Ohshima, and K. Kato, J. Appl. Crystallogr. **28**, 599 (1995).
[10] Y. Uchida, Y. Kanke, J. S. Lord, and P. C. Riedi, J. Magn. Magn. Mater. **140–144**, 163 (1995).
[11] T. Naka, T. Matsumoto, Y. Kanke, and K. Murata, Physica B **206&207**, 853 (1995).
[12] D.-K. Seo and M.-H. Whangbo, J. Am. Chem. Soc. **118**, 3951 (1996).
[13] O. Mentre, A.-C. Dhaussy, F. Abraham, and H. Steinfink, J. Solid State Chem. **130**, 223 (1997).
[14] M. Iwata and Y. Ishibashi, J. Phys. Soc. Jpn. **67**, 691 (1998).
[15] A. Akiba, H. Yamada, R. Matsuo, Y. Kanke, T. Haeiwa, and E. Kita, J. Phys. Soc. Jpn. **67**, 1303 (1998).
[16] F. Haberey and M. Velicescu, Acta Crystallogr., Sect. B: Struct. Crystallogr. Cryst. Chem. **30**, 127 (1974).
[17] X. Obradors, A. Collomb, J. Pannetier, A. Isalgue, J. Teyada, and J. C. Joubert, Mater. Res. Bull. **18**, 1543 (1983).
[18] M. C. Cadée and D. J. W. Ijdo, J. Solid State Chem. **52**, 171 (1985).
[19] M. C. Cadée and D. J. W. Ijdo, J. Solid State Chem. **36**, 314 (1981).
[20] D. Verdoes, H. W. Zandbergen, and D. J. W. Ijdo, Mater. Res. Bull. **22**, 1 (1987).
[21] W. D. Townes, J. H. Fang, and A. J. Perotta, Z. Kristallogr. **125**, 437 (1967).
[22] X. Obradors, A. Collomb, M. Pernet, D. Samaras, and J. C. Joubert, J. Solid State Chem. **56**, 171 (1985).
[23] Y. Kanke, E. Takayama-Muromachi, Y. Uchida, K. Kato, and S. Takekawa, J. Solid State Chem. **95**, 438 (1991).
[24] S. Tamura and Y. Kanke, J. Phys. Soc. Jpn. **60**, 4386 (1991).
[25] Y. Kanke, F. Izumi, Y. Morii, S. Funahashi, and K. Kato, J. Solid State Chem. **104**, 319 (1993).
[26] Y. Hata, Y. Kanke, E. Kita, H. Suzuki, and G. Kido, J. Appl. Phys. **85**, 4768 (1999).
[27] Y. Kanke, Y. Hata, E. Kita, and K. Kato (unpublished).
[28] H. Kato, M. Kato, K. Yoshimura, and K. Kosuge (private communication).
[29] S. Yamaoka, M. Akaishi, H. Kanda, T. Osawa, T. Taniguchi, H. Sei, and O. Fukunaga, J. High Pressure Inst. Jpn. **30**, 249 (1992).
[30] M. Akaishi, H. Kanda, and S. Yamaoka, J. Cryst. Growth **104**, 578 (1990).
[31] M. Akaishi, H. Kanda, and S. Yamaoka, Science **259**, 1592 (1993).
[32] H. Okada, N. Kinomura, S. Kume, and M. Koizumi, Mater. Res. Bull. **13**, 1047 (1978).
[33] W. Abriel, F. Rau, and K.-J. Range, Mater. Res. Bull. **14**, 1463 (1979).
[34] B. A. Frenz and Associates Inc. and Enraf-Nonius, Structure Determination Package, 4th ed., 1985.
[35] K. Kato, anonymous twin refinement program, 1998.
[36] *International Tables for X-Ray Crystallography*, edited by A. J. C. Wilson (Kluwer Academic, Dordrecht, 1992), Vol. C.
[37] Additional material to this paper can be ordered referring to the No. CSD-410568 (295 K) and No. CSD-410569 (154 K), name of the author, and citation of the paper at the Fachinformationszentrum Karlsruhe, Gesellschaft für wissenschaftlich-technische Information mbH, D-76344 Eggenstein-Leopoldshafen, Germany.
[38] K. Kato (private communication).
[39] Y. Uchida, Y. Onoda, and Y. Kanke (unpublished).
[40] J. P. Renard, M. Verdaguer, L. P. Regnault, W. A. C. Erkelens, J. Rossat-Mignod, and W. G. Stirling, Europhys. Lett. **3**, 945 (1987).
[41] F. D. M. Haldane, Phys. Rev. Lett. **50**, 1153 (1983).
[42] M. Troyer, H. Tsunetsugu, and D. Würtz, Phys. Rev. B **50**, 13 515 (1994).
[43] M. Azuma, Z. Hiroi, M. Takano, K. Ishida, and Y. Kitaoka, Phys. Rev. Lett. **73**, 3463 (1994).
[44] H. Iwase, M. Isobe, Y. Ueda, and H. Yasuoka, J. Phys. Soc. Jpn. **65**, 2397 (1996).
[45] Y. Sasago, M. Hase, K. Uchinokura, M. Tokunaga, and N. Miura, Phys. Rev. B **52**, 3533 (1995).
[46] A. Arrott and J. E. Noakes, Phys. Rev. Lett. **19**, 786 (1967).
[47] Y. Takahashi, J. Phys. Soc. Jpn. **55**, 3553 (1986).
[48] For a review, see T. Moriya, *Spin Fluctuations in Itinerant Electron Magnetism* (Springer-Verlag, Berlin, 1985).
[49] K. Shimizu, H. Maruyama, H. Yamazaki, and H. Watanabe, J. Phys. Soc. Jpn. **59**, 305 (1990).
[50] A. D. Shannon, Acta Crystallogr., Sect. A: Cryst. Phys., Diffr., Theor. Gen. Crystallogr. **32**, 751 (1976).
[51] H. F. Pen, J. van den Brink, D. I. Khomskii, and G. A. Sawatzky, Phys. Rev. Lett. **78**, 1323 (1997).
[52] R. W. Powell, Philos. Mag. **44**, 772 (1953).